Microturbulence, heat, and particle fluxes in JET and DIII-D ITB plasmas with highly reversed magnetic shear

R.V.Budny[a], R.Andre[a], C.D.Challis[b], W.Dorland[c], R.Dux[d], D.R.Ernst[e], C.Giroud[f], C.W.Gowers[b], C.M.Greenfield[g], N.Hawkes[b], G.W.Hammett[a], W.A.Houlberg[i], T.C.Luce[g], M.A.Makowski[h], D.Mikkelsen[a], M.Murakami[i], R.Prentice[b], G.Staebler[g], B.Stratton[a], M.R.Wade[i], W.P.West[g], and contributors to the EFDA-JET and DIII-D work programs
[a] *Princeton Plasma Physics Laboratory, P.O. Box 451, Princeton, NJ 08543, USA,* [b] *UKAEA Science Centre, Abingdon, Oxfordshire, OX14 3DB, UK,* [c] *Univ. of Md., College Park, MD, USA,* [d] *MPI fur Plasmaphysik, Garching, GR,* [e] *MIT, Cambridge MA, USA,* [f] *FOM-Rijnhuizen, Ass. Euratom-FOM, TEC, NL,* [g] *General Atomics, San Diego, CA, USA,* [h] *LLNL, Livermore, CA, USA,* [i] *ORNL, Nashville, TN, USA*

Introduction - Practical tokamak reactors will need to maintain high T_i and $n_D \simeq n_T$ in the core for long durations. These conditions will necessitate low energy transport, low impurity concentrations, and high bootstrap current. Large extrapolations from present experiments are needed to predict performance. A number of approaches are being used for these extrapolations including: 1) dimensionless scaling arguments, 2) empirical scaling, and 3) physics-based simulations of anomalous transport.

Microturbulence is a leading candidate for the cause of anomalous transport in present tokamak plasmas. Much progress has been made in refining both measurements and simulations of microturbulence. One key result of the simulations has been highlighting the nonlinear dependence of plasma fluxes on ∇T_i. Since burning plasmas need high core T_i, limited ∇T_i imply large plasma radii or high edge temperatures in a reactor.

To simulate microturbulence, generally the gyro-averaged Vlasov equation is solved using either gyrofluid or gyrokinetic techniques. Although solutions to the gyrofluid equations tend to be relatively easy and fast, the gyrokinetic approach includes more physics, such as Landau resonances, and avoids uncertainties concerning closure of the moment equations, Also a large number of Fourier moments for the modes can be included.

Both particle-in-cell and continuum approaches have been used for solving the gyrokinetic equations. The simulation domain size ranges from a single flux-tube to a whole torus. In this paper, the GS2 [1] continuum flux-tube code is chosen since it is the only gyrokinetic code capable of treating a large number of plasma species in a realistic geometry. It is a comprehensive code simulating turbulence and turbulently-driven fluxes in either a linear approximation, or a nonlinear generalization. Linear estimates of drift-wave turbulence have been used to calibrate models for extrapolating present plasma performance to burning plasmas. Further work is needed to substantiate these predictive models.

This paper presents nonlinear simulations of heat and particle fluxes in two Advanced Tokamak plasmas. The microturbulently-driven fluxes of multiple species, including high Z impurities are outward. The fluxes are strongly suppressed in the regions of strong negative magnetic shear, consistent with measurements. However, the calculated fluxes saturate at values much higher than the measured values in regions of less negative and positive magnetic shear. They are saturated by zonal flows and eddies, interspersed with large, brief bursts of heat and particle fluxes. Effects, ignored in the simulations, which might explain the discrepancy are: 1) the strong externally-driven flow shear, and 2) β-driven electromagnetic fluctuations.

Plasmas studied - The JET plasma [2] had highly reversed (i.e., non-monotonic) q with a current hole [3] formed by 2.1 MW LHCD and current rampup. The auxiliary heating consisted of 17.1 MW D-NBI and 4.0 MW H-minority ICRH. The co-orientation of the NBI resulted in a carbon toroidal rotation rate of 230 krad/s in the core, corresponding to Mach numbers of 1.7 for the carbon impurity, and 0.7 computed for the thermal D. Several Internal Transport Barrier phases (defined by regions of large R/L_{T_i} in the core) occurred. In the final phase, the ITB grew to a large radius shortly before the plasma terminated with a disruption. The analysis time (6 s) was chosen to be 112 msec after the formation of the last ITB, during its expansion.

The DIII-D plasma [4] had a reversed q profile formed using off-axis ECCD/ECH. The auxiliary heating consisted of 7.5 MW D-NBI. The co-orientation of the NBI resulted in a carbon toroidal rotation rate of 170 krad/s in the core, with Mach numbers of 1.0 for the

carbon impurity, and 0.4 computed for the thermal D. It was relatively steady state until a neoclassical tearing mode occurred. Time-evolutions of the thermal deuterium T_i for both plasmas, at fixed values of the toroidal flux label $x \equiv \sqrt{\text{normalized toroidal flux}}$, are shown in Fig. 1. Profiles of the temperatures at the analysis time (2.7 s) are shown in Fig. 2. Reversed q profiles, also shown in Fig. 2, were measured using MSE. These q profiles are very challenging for the MHD equilibrium solvers, so there are uncertainties in the calculated flux surfaces, especially in the core.

Both plasmas had high confinement and apparent accumulation of high Z impurities within the ITB. It is important to determine if reduction of microturbulence is necessarily correlated with large impurity densities or inward fluxes. In the JET plasma, Be, C, Ne, and Ni density profiles were derived from charge-exchange and soft X-ray emission measurements. In the DIII-D plasma, C, Cu, and Ni density profiles were derived from charge-exchange, bremsstrahlung, and spectroscopy measurements. The analysis of the data does not compensate for the neoclassical effects that are expected to cause poloidal anisotropies in the impurity densities, especially at high Mach numbers.

A summary of plasma parameters is given in Table I. The TRANSP plasma analysis code [5] was used to study transport in the plasmas. Heat fluxes are computed from measured plasma profiles and calculated heat depositions. The conducted plus convected heat fluxes given in Table I are lower than the total heating powers since radiation, charge-exchange losses, and dW/dt terms have been subtracted. Resulting profiles of χ_i are relatively low in the negative magnetic shear region, and increase to large values ($\simeq 8m^2/s$) near the top of the pedestals. The ratio of χ_i to $\chi_{neoclass}$ rises steadily from low values in the core to greater than 100 near the pedestal. The minimum values of q occurs near x=0.47 and 0.55 at the analysis times for the plasmas, and are near the locations of the foot of the ITB. A_{plasma} is the area of the flux surface at x, the magnetic shear is $\hat{s} \equiv (r/q)dq/dr$, $\alpha \equiv -Rq^2|\nabla\beta|$, and $\rho_* \equiv \rho_i/L_{T_i}$. Note the large values of the parameter R/L_{Ti} that drives drift waves. γ_{ExB} is the Hahm-Burrell flow shearing rate [6] calculated from the measured toroidal rotation, pressure, and neoclassical poloidal rotation. The particle fluxes are computed from the densities and sources. The fluxes of impurities are derived from the time-evolutions, of their densities, averaged over $\simeq 0.5s$.

	JET	51976		DIII-D	111203	
x (≈r/a)	0.30	0.40	0.60	0.45	0.60	0.75
A_{plasma} [m^2]	44.0	58.9	87.0	26.2	33.5	40.5
$\hat{s}$	-2.61	-0.83	0.63	-0.61	0.57	1.67
α	6.5	1.8	0.7	2.0	1.0	1.0
R/L_{T_i}	7.8	12.9	11.0	7.9	4.6	1.9
ρ_* [10^{-2}]	1.4	1.7	0.8	1.9	2.5	0.5
E_r [kV/m]	40	65	55	20	25	30
γ_{ExB}[krad/s]	40	80	60	25	15	5
Q_e [MW]	1.5(-0.0)	1.9(+0.0)	1.7(+0.0)	3.4(-0.0)	4.2(-0.0)	4.2(+0.0)
Q_{ion} [MW]	2.8(+2.2)	3.5(+0.5)	5.9(+0.1)	2.6(+0.5)	3.2(+0.1)	3.4(-0.0)
Γ_e [$10^{20}/s$]	1.9(+0.2)	2.6(-0.0)	4.0(-0.0)	5.6(+2.4)	7.4(+0.7)	9.4(-0.3)
Γ_D [$10^{20}/s$]	3.9(+0.2)	4.2(+0.0)	5.0(+0.2)	6.1(+1.6)	7.8(+0.9)	5.2(+0.9)
Γ_C [$10^{18}/s$]	-3.0(-1.1)	-5.0(-1.7)	-14.0(-7.8)	-1.0(-18.0)	-3.0(-3.6)	-4.0(-28.0)
Γ_{Ne} [$10^{18}/s$]	-1.0(+0.2)	-1.6(+0.0)	-6.0(-1.3)			
Γ_{Ni} [$10^{17}/s$]	-7.0(+1.8)	-12.0(+0.7)	-20.0(+1.4)	-0.3(+2.0)	-0.4(+1.5)	-0.4(+0.2)
Γ_{Cu} [$10^{15}/s$]				-6.0(+42.0)	-7.0(+40.0)	-8.0(+5.0)

Table 1: *Summary of the JET and DIII-D plasma parameters at the analysis locations*

Results - The flux values in parentheses in Table 1 are the neoclassical values predicted by the NCLASS code [7]. The neoclassical results for carbon show inward fluxes, in qualitative agreement with the measurements. Those for the higher Z impurities are generally outward, contrary to the measurements, but the uncertainties in both the measurements and neoclassical calculations for high Z impurities are large. NCLASS does not completely include the temperature screening effects expected in the Pfirsch-Schluter regime at large impurity collisionality.

The linear and nonlinear GS2 runs were performed assuming non-adiabatic electrons in the electrostatic approximation. The Miller approximation [8] was used to input realistic geometries for the shaped flux surfaces, allowing computation of the second-stability effects of α stabilization. Collisions were modeled using energy-dependent Lorentz collision operators. Both linear and nonlinear runs were done using 6 species for the JET plasma: e^-, thermal-D, NBI-D, C, Ne, and Ni, but neglecting the relatively small measured Be density. For the DIII-D plasma, five species were used for the the inner two radii: e^-, thermal-D, NBI-D, C, and Ni. The measured Cu density was relatively low. Both the Ni and Cu densities were relatively low at the outer radius (x=0.75), and thus ignored. The GS2 runs were performed on an IBM SP computer. The nonlinear runs used between 512 and 1024 parallel processors. The plasma region simulated by the nonlinear runs was a rectangle at the largest major radius with length (in the radial direction) and width (in the transverse, poloidal direction) typically 30-50 ρ_i. The largest value of the mode wavenumbers in the transverse (poloidal) direction was $|k_y| \leq 3/\rho_i$, so ETG modes are ignored.

Previous linear results from GS2 for the fastest linear growth rate γ_{lin} for ITG turbulence indicate that the ratio $|\gamma_{ExB}/\gamma_{lin}|$ correlates with reductions of the local χ_i [9], qualitatively consistent with the Waltz criterion [10]. For the JET plasma, the expansion of the region where this ratio reduces to near unity correlates with the expansion of the foot of the ITB. ITG modes are computed to be suppressed ($\gamma_{lin} < 0$) in regions with sufficiently negative $\hat{s}$.

The nonlinear GS2 runs start from an initial low level of turbulence, and calculate either mode decay, or growth then saturation with bursts. Zonal flows play significant roles in the saturation. As with the linear runs, these simulations also predict that the microturbulence is strongly suppressed when $\hat{s}$ is sufficiently negative. Figure 3-a shows the heat fluxes for the JET plasma at the inner radius (where $\hat{s} = -2.61$) dropping below 1 W within 30 μsec. In contrast, the computed heat fluxes at the next radius, x=0.4 (where $\hat{s} = -0.83$), shown in Fig. 3-b are very large. Near the end of this run the average deuterium heat flux is 150 MW, in contrast to the measured value of $Q_{ion} = 3.5$ MW in Table I. Figure 3-b shows an example of a typical burst of the heat and particle fluxes seen with durations of about 30-100 μsec. Similar bursts have been measured in TFTR plasmas with negative $\hat{s}$ [11]. For the DIII-D plasma at the inner radius with comparable $\hat{s}$ ($= -0.61$), the microturbulence was suppressed. The JET plasma had a much larger L/R_{Ti} at x=0.40 than the DIII-D plasma at x=0.45. At the largest radii studied, collisionless trapped electron mode instabilities are seen in the calculations, with simulated particle and heat fluxes much higher than the measured values. The simulated particle fluxes show the same qualitative features of the heat fluxes. The direction of the microturbulent-driven fluxes of the impurities is outward. This suggests that the measured accumulations inside the ITB are due to neoclassical effects, not microturbulence.

Discussion - Previous nonlinear GS2 results [12] for a DIII-D L-mode plasma gave fluxes higher than measured by factors of 2-4. The simulated nonlinear turbulent-driven heat and particle fluxes for the Advanced Tokamak plasmas studied are either strongly suppressed (near the core), or are higher than the experimental values by several orders of magnitude. The measurements and TRANSP analysis have errors and uncertainties, as do the gyrokinetic theory and GS2 code. Although the fluxes depend very sensitively on R/L_{Ti}, the large reductions needed to reconcile the fluxes do not appear to be realistic. The external NBI-driven γ_{ExB} shearing rate, dominated by the sheared v_{tor} are large, and not taken into account in the nonlinear GS2 calculations. These are expected to couple stable with unstable modes, and may result in lower fluxes. Also, α-stabilization of magnetic fluctuations can stabilize in certain regimes [13]. These have not been investigated yet for Advanced Tokamak plasmas. Another possibility is that microturbulence shifts local plasma profiles to more stable values. Slight changes in various profiles and gradients can have large effects on the microturbulence fluxes. A gyrokinetic predictive transport model might be needed to accurately model such effects.

*This work has been conducted in part under the European Fusion Development Agreement and supported in part by the US DoE Contract No. DE-AC02-76CH03073.

[1] see http://gs2.sourceforge.net
[2] C.D. Challis, Yu Baranov, A. Bécoulet, *et al.*, Plasma Phys. Control. Fusion **44** (2002), 1031
[3] B.C. Stratton, *et al.*, 19th IAEA Fusion Energy Conf., Lyon, IAEA-CN-94/EX/C3-1Rb
[4] M. Murakami, M.R. Wade, J.C. DeBoo, C.M. Greenfield, *et al.*, Phys. Plasmas **10** (2003), 1691

[5] R.V. Budny, M.G. Bell, A.C. Janos, *et al.*, Nuclear Fusion **35** (1995) 1497
[6] T.-S. Hahm and K. Burrell, Phys. Plasmas **2** (1995), 1648
[7] M.R. Wade, W.A. Houlberg, and L. Baylor, Phys. Rev. Letters **84** (2000), 282
[8] R.L. Miller, M.S. Chu, J.M. Green, *et al.*, Phys. Plasmas **5** (1998) 973
[9] R.V. Budny, R. Andre, A. Bécoulet, *et al.*, Plasma Phys. Control. Fusion **44** (2002), 1215
[10] R.E. Waltz, G.D. Kerbel, J. Milovich, Phys. Plasmas **1** (1994), 2229
[11] E. Mazzucato, S.H. Batha, M. Beer, *et al.*, Phys. Review Lett **77** (1996), 3145
[12] D.W. Ross and W. Dorland, Phys. Plasmas **9** (2002), 5031
[13] P.B. Snyder, G.W. Hammett, Phys. Plasmas **8** (2001), 744

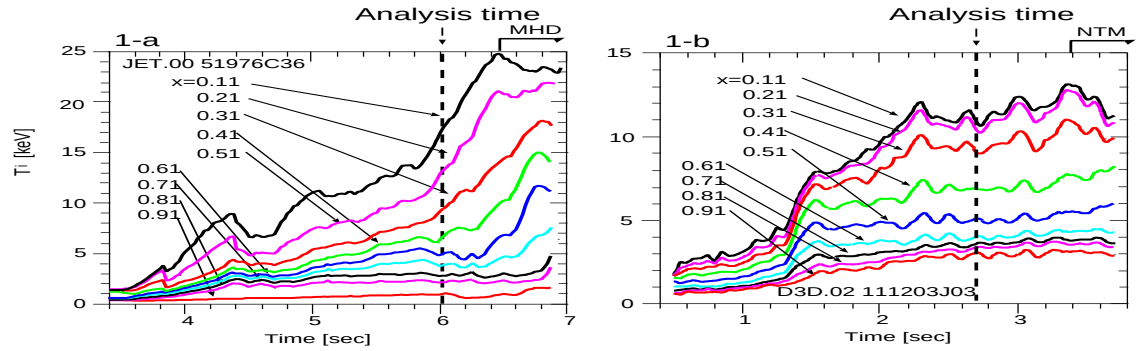

Fig. 1 - Time evolutions of ion temperatures in the a) JET and b) DIII-D plasmas

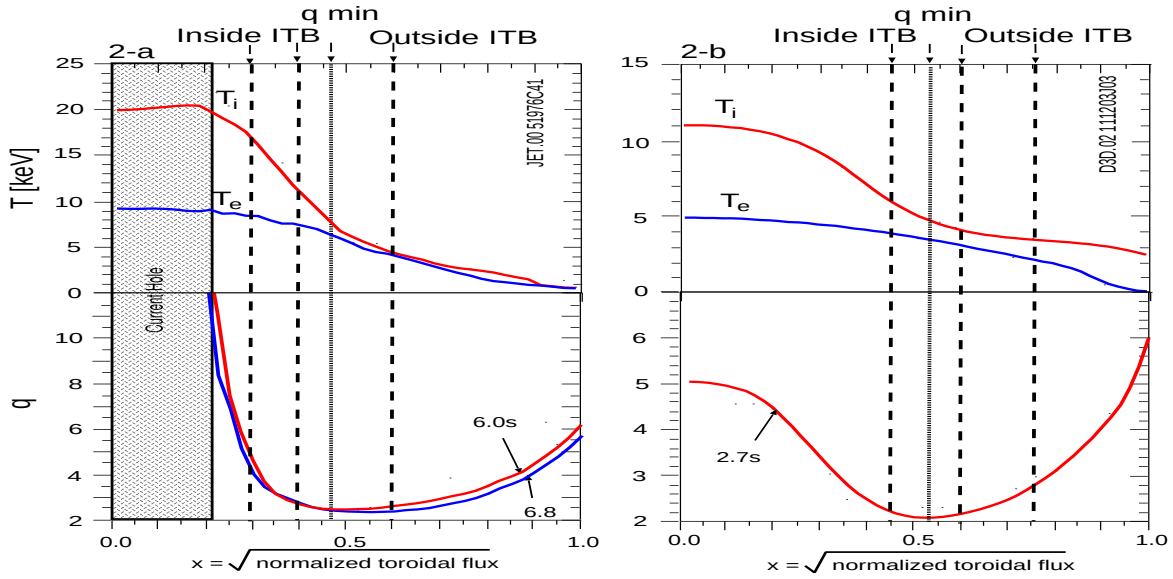

Fig. 2 - Measured profiles of temperatures and q in a) JET and b) DIII-D plasmas

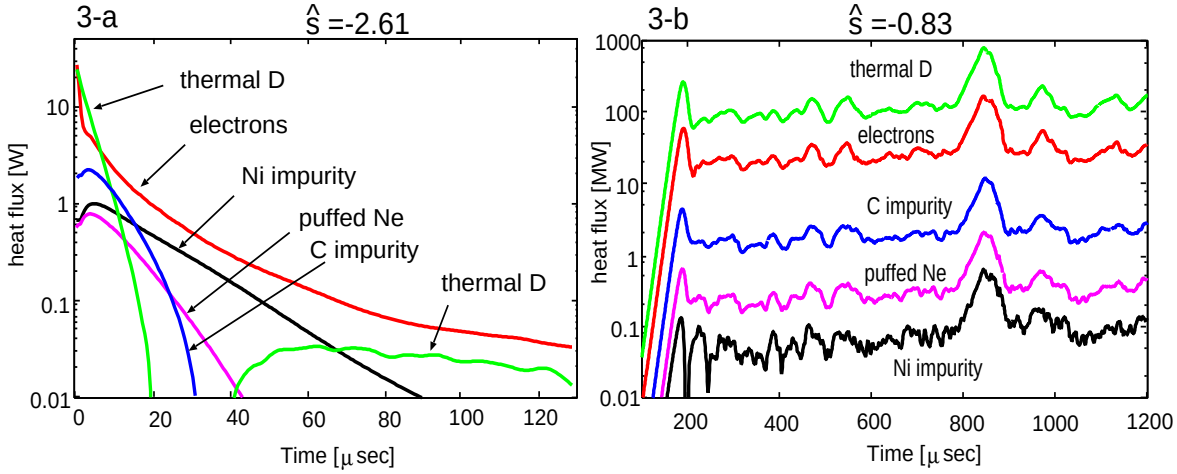

Fig. 3 - Nonlinear GS2 results for heat flux in the JET plasma at a) x=0.3, and b) x=0.4